Chemical Science

ROYAL SOCIETY OF CHEMISTRY

EDGE ARTICLE

View Article Online
View Journal | View Issue

Cite this: *Chem. Sci.*, 2025, **16**, 22769

All publication charges for this article have been paid for by the Royal Society of Chemistry

Understanding the formation mechanism of crystalline hydrated polymorphs of carbonic acid from CO_2 clathrate hydrate

Selene Berni, [ac] Demetrio Scelta, [*ab] Sebastiano Romi, [ac] Samuele Fanetti, [ab] Frederico Alabarse, [d] Bjorn Wehinger[e] and Roberto Bini [*abcf]

Received 24th March 2025
Accepted 22nd October 2025

DOI: 10.1039/d5sc02241j

rsc.li/chemical-science

Carbon dioxide (CO_2) and water (H_2O) icy mixtures, together with a few other simple molecules, have a prominent role in astrochemical processes. The formation of the solid 1 : 1 CO_2 : H_2O adduct, carbonic acid (H_2CO_3), has been long studied because of its importance in the biological and geochemical domains. Our recent discovery of a novel, highly reproducible synthetic path to obtain crystalline hydrated H_2CO_3 polymorphs from low temperature compression of CO_2 clathrate hydrate highlighted the role of pressure in the chemistry of crystal ices. Herein, we report an extensive study about the reaction mechanism leading to this synthesis, unveiling a multi-step temperature-governed process that involves the formation of carbonic acid molecules starting from about 200 K and their organisation in a crystalline lattice at temperatures close to 270 K. In addition, the essential role played by the clathrate in the formation of crystalline carbonic acids is clearly highlighted, while the entire process meticulously mimics what can occur during the subduction of icy materials.

Introduction

Ices are widespread across the solar system, with an increasing presence and consequently a more prominent role as we move farther from the Sun. Water ice is the most abundant frozen molecule followed by, depending on the nature and origin of planets and satellites, methane, ammonia, carbon dioxide, carbon monoxide, nitrogen, methanol and others.[1] These volatiles generally produce icy mixtures existing in many different forms. One component can be randomly dispersed as isolated molecules or small clusters within the crystalline or amorphous domains of the prevalent species, but larger crystalline mixed domains are also possible as well as hydrate phases.[2] Among the latter, an important class of crystalline water based structures thought to be common in the interior of several planets and satellites are clathrate hydrates.[3] In these crystalline polymorphs, water molecules are hydrogen bonded to form polyhedral cages stabilised by the repulsive interactions with the guest molecules hosted inside, and bonded together to create a regular three-dimensional array. We focus our attention on carbon dioxide, which is the most abundant carbon bearing species in the solar system, and is present almost everywhere from Mercury to the trans-Neptunian objects.[4–8] Despite the lack of spectral evidence for the presence of CO_2 clathrate hydrates on these planets' outermost layers, from a thermodynamic point of view, they are stable at (or close to) the surface of many cold natural objects: in the crust, in the underlying oceans or in ice caps.[9]

These icy mixtures are thought to be, at least in part, the starting materials from which many organic molecules detected on the surfaces or in the atmospheres are derived.[10–12] Among the species having an astrobiological relevance, carbonic acid occupies a prominent position playing an important role in many biological and geochemical processes.[13,14] Its presence has been suggested in different astronomical environments characterised by the simultaneous presence of water ice and CO_2 (ref. 15–19), but only recently the carbonic acid molecule has been detected in the Galactic Center.[20] Many laboratory experiments[21] have reported carbonic acid as a major product of low temperature irradiation of icy H_2O/CO_2 mixtures by protons,[22,23] vacuum UV photons,[24,25] and electrons.[26,27] Besides these energetic processes, the formation of H_2CO_3 was also reported in low temperature reactions of CO molecules with non-energetic hydroxyl radicals.[28] All these experiments mimic the conditions that can be found at the surfaces of planets and

[a]*LENS, European Laboratory for Non-linear Spectroscopy, Via N. Carrara 1, I-50019 Sesto Fiorentino, Firenze, Italy. E-mail: scelta@lens.unifi.it; roberto.bini@unifi.it*

[b]*ICCOM-CNR, Institute of Chemistry of Organo Metallic Compounds, National Research Council of Italy, Via Madonna del Piano 10, I-50019 Sesto Fiorentino, Firenze, Italy*

[c]*Dipartimento di Chimica "Ugo Schiff" dell'Università degli Studi di Firenze, Via della Lastruccia 3, I-50019 Sesto Fiorentino, Firenze, Italy*

[d]*ELETTRA, Elettra Sincrotrone Trieste S.C.p.A, AREA Science Park, Basovizza, Trieste, 34149, Italy*

[e]*ESRF, European Synchrotron Radiation Facility, 71 Avenue des Martyrs, CS40220, 38043 Grenoble Cedex 9, France*

[f]*INO-CNR, Istituto Nazionale di Ottica, Via N. Carrara 1, I-50019 Sesto Fiorentino, Firenze, Italy*

satellites overlooking all the reactions that can be induced by a pressure increase. The latter can be roughly divided into two main classes depending on the temperature conditions: moderate pressures and low temperatures are relevant in geodynamic crustal processes, while high pressures and high temperatures enclose reactions occurring in the depth or in surface impact events.[29,30] To the second class belong two recent experiments where a fluid mixture of H_2O and CO_2 was heated at pressures of few gigapascals resulting in the synthesis of crystalline carbonic acid. In one case, the fluid mixture was laser heated in a diamond anvil cell (DAC) up to 1500 °C between 1.5 and 4.6 GPa;[31] milder temperature conditions, 150 °C, were instead employed for heating resistively the diamond anvil cell at 6.5 GPa.[32] All these conditions are consistent with those encountered in subsurface oceans,[33,34] thus demonstrating that alternative routes to photoirradiation are feasible. In one of these experiments, Abramson *et al.* were able to grow single crystals, which allowed the refinement of the crystal structure to a triclinic unit cell ($P\bar{1}$ space group) containing two water and two carbonic acid molecules.[35] This is the first identified crystal structure, which they labeled as S3, containing the H_2CO_3 molecule, since the compound synthesised at low temperature and low pressure, and indicated as β, has been characterised only by spectroscopic techniques.[22,36–39] Another phase, labelled as α, was also claimed on the basis of spectroscopic data[40,41] but later demonstrated to be a monomethyl ester of H_2CO_3.[42,43] Recently, a high-pressure (1.85 GPa) neutron-diffraction study on D_2CO_3 has suggested an anhydrous monoclinic structure, with the space group $P2_1/c$ and $Z = 4$, where the molecules form dimers with a symmetric double H-bond, leading to the formation of molecular stripes along the monoclinic b axis.[44] Computational studies report a huge stability of anhydrous crystalline carbonic acid up to pressures of a few Mbars, which are characteristic of the interiors of giant planets, all of them agreeing on an orthorhombic $Cmc2_1$ crystal structure.[45–47] All these studies evidence a marked tendency of carbonic acid to polymorphism, also considering the possibility to have anhydrous or hydrate phases.

Recently, we have reported the formation of three different carbonic acid crystalline polymorphs through the low temperature compression of CO_2 clathrate hydrate.[48] These results are particularly important because the reaction occurs without the need for high temperature or irradiation, mimicking the conditions that can characterise a subduction process. The different crystalline polymorphs were detected after the loading and the sealing in a DAC of CO_2 clathrate hydrate at about 100 K. The pressure to which the sample is subjected during this process depends on the force applied for sealing the sample and on the diamonds employed, so that it can vary from few kbars to some GPa. Once the sample reached ambient temperature, we encountered different scenarios depending on the pressure value. Below 2.7 GPa, we found only the characteristic Raman features of liquid (or solid) H_2O and CO_2, thus indicating the decomposition of clathrate hydrate. Above 2.7 GPa, we instead observed the formation of different polymorphs of carbonic acid. Between 2.7 and 4.8 GPa, the Raman spectrum unambiguously indicates a crystal structure different from those found so far, while above 4.8 GPa we always obtained an amorphous phase. The latter phase converted into a crystalline structure once decompressed between 5 and 7 GPa at temperatures of 300 and 380 K, respectively. The diffraction pattern of this phase, which we called ε, was refined using the $P\bar{1}$ space group proposed by Abramson *et al.*[35] In addition, this structure also accounts well for the observed lattice phonon spectrum and for the presence of O–H stretching modes due to water molecules. This phase is extremely stable upon compression (up to at least 50 GPa) and heating (about 500 K). The structure forming between 2.7 and 4.8 GPa, which we called ε_m, presents a different diffraction pattern, a lower number of lattice phonon modes and no O–H stretching bands, indicating an anhydrous structure or water molecules arranged in a disordered manner. In addition, this phase irreversibly converts into the ε phase upon heating above 400 K, thus clarifying its metastable character. Different questions arise from this study. First of all, which mechanism leads to the formation of carbonic acid molecules, and especially to their arrangement in a crystalline ordered structure? Is it due to the anisotropic stress to which the CO_2 clathrate hydrate is subjected during the low temperature compression or is it intrinsic to the density conditions realised? Does the formation of carbonic acid require CO_2 clathrate hydrate as a starting material or a CO_2–H_2O icy mixture is sufficient?

We have tried to answer these questions by gradually compressing CO_2 clathrate hydrate crystals along specific low temperature isotherms in order to unveil the conditions of carbonic acid molecule formation and of their arrangement in a crystal. In addition, the structural characterisation of the ε_m phase has been achieved, showing that it is a kinetically trapped intermediate structure toward the ε phase.

Results and discussion

The formation mechanism of crystalline carbonic acid polymorphs

In order to study the conditions leading to the formation of crystalline H_2CO_3 from CO_2 clathrate hydrate, we loaded the latter into membrane driven diamond anvil cells at about 77 K, as described in the Methods section (Section SI-1 of the SI).[49] All the loadings generally ended at a final pressure, at ambient temperature, between 3.5 and 4.5 GPa. As expected, upon closing the DAC, the pristine clathrate hydrate underwent a transformation to a mixture of ε_m-H_2CO_3, CO_2-I and ice-VII,[48] once the ambient temperature was recovered. The samples were then decompressed to pressures between 0.1 and 0.5 GPa, where both H_2O and CO_2, the only compounds still present after H_2CO_3 decomposition at about 2.7 GPa, were fluids. The decompressed samples were then subjected to isobaric cooling down to temperature conditions, where depending on the pressure the CO_2 clathrate hydrate was expected to start nucleating.[50–52]

Fig. 1, panel a, shows a portion of the CO_2 clathrate hydrate phase diagram (orange lines) superimposed onto those of pure H_2O (dashed blue lines) and CO_2 (purple line). The red star marks the p,T conditions under which the clathrate hydrate

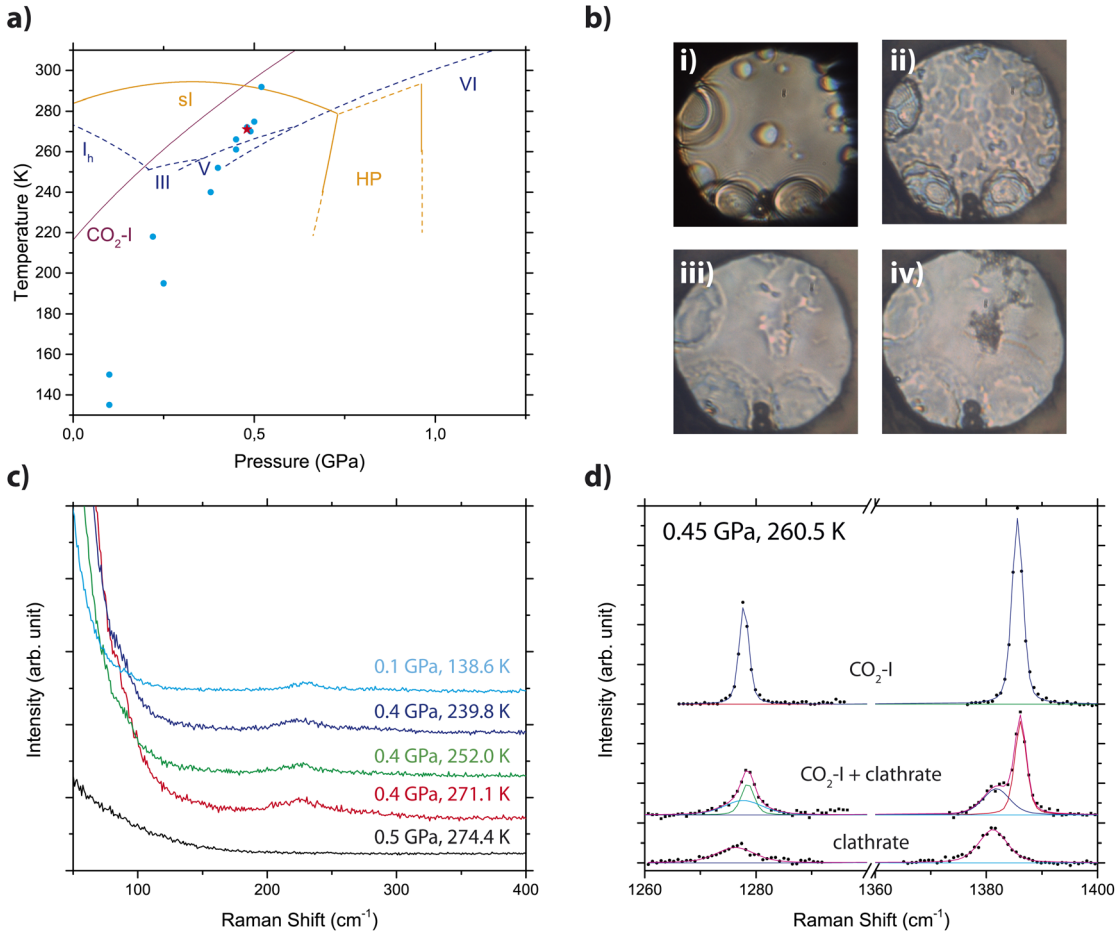

Fig. 1 Formation of CO_2 clathrate hydrate during the isobaric cooling of a fluid mixture of H_2O and CO_2. Panel (a) phase diagrams of CO_2 clathrate hydrate (orange, from data of Bollengier *et al.*[51]), H_2O (blue dashed lines, from ref. 56) and CO_2 (solid purple line, from ref. 57). The cyan circles highlight the experimental points taken upon cooling, while the red star marks *p*,*T* conditions under which the CO_2 clathrate hydrate nucleation occurs. Panel (b) microphotographs of a typical sample during crystal nucleation: (i) at 0.52 GPa and 292 K; (ii) at 0.44 GPa and 271.5 K; (iii) at 0.38 GPa and 239.9 K; (iv) at 0.1 and 135.1 K. Panel (c) Raman spectra acquired in the lattice phonon mode region upon cooling. Panel (d) Raman spectra acquired in the Fermi resonances Ω^+ and Ω^- in CO_2, mixed CO_2 and CO_2 clathrate, and pure CO_2 clathrate regions at 0.45 GPa and 260.5 K. Spectra are vertically shifted for the sake of clarity.

described below is obtained upon cooling (0.48 GPa and 271 K). As it can be seen from the sequence of microphotographs reported in panel b of Fig. 1, the formation of CO_2 clathrate hydrate is accompanied by an evident change of aspect in the sample, whose texture transforms from being fully transparent when it is in the fluid phase (i) to the appearance of opaque solid regions (ii), which further extend until they occupy the entire sample area (iii and iv). The formation of CO_2 clathrate hydrate is attested by Raman spectra (panel c in Fig. 1) collected upon cooling the sample. Once the sample changes its visual aspect, a lattice phonon mode, perfectly compatible with a lattice phonon mode of sI clathrate hydrates, appears at about 225 cm^{-1}.[51,53] Contextually, in different regions of the sample, different spectra related to the CO_2 Fermi resonance[54,55] are observed, as shown in panel d of Fig. 1. The two Fermi bands Ω^+ and Ω^- for pure CO_2, respectively, centred at 1385.7 and 1277.7 cm^{-1} (with a $\Delta\nu$ of about 108 cm^{-1}, as expected for pure CO_2), are accompanied by two weaker and broader low frequency shoulders centred at 1381.1 and 1276.2 cm^{-1} (with a $\Delta\nu$ of about 105 cm^{-1}), featuring FWHMs compatible with the ones reported for CO_2 clathrate hydrate (6 and 8 cm^{-1},[51] to be compared to the sharper bands from pure CO_2 Fermi resonances, having FWHMs of about 2.5–3 cm^{-1}) and that we therefore assigned to the CO_2 encaged in the sI clathrate hydrate. Pure CO_2 is detected in the round-shaped regions of the sample close to the gasket border, where in fact only the Fermi resonance bands for pure CO_2 are observed. In the same way, where no CO_2 excess is present, only the Ω^+ and Ω^- bands related to CO_2 in clathrate hydrate are found.

Once the CO_2 clathrate hydrate nucleated, the sample was cooled down to a target temperature (in this case, 130 K). This temperature was chosen to mimic the condition under which the clathrate samples, synthesised *ex situ*, were loaded into the DAC. Once the temperature of 130 K was reached, the samples were isothermally compressed up to the target pressure (3.5 GPa) and then isobarically heated to room temperature to fully reproduce the *p*,*T* cycle to which the samples were subjected to after a typical loading.

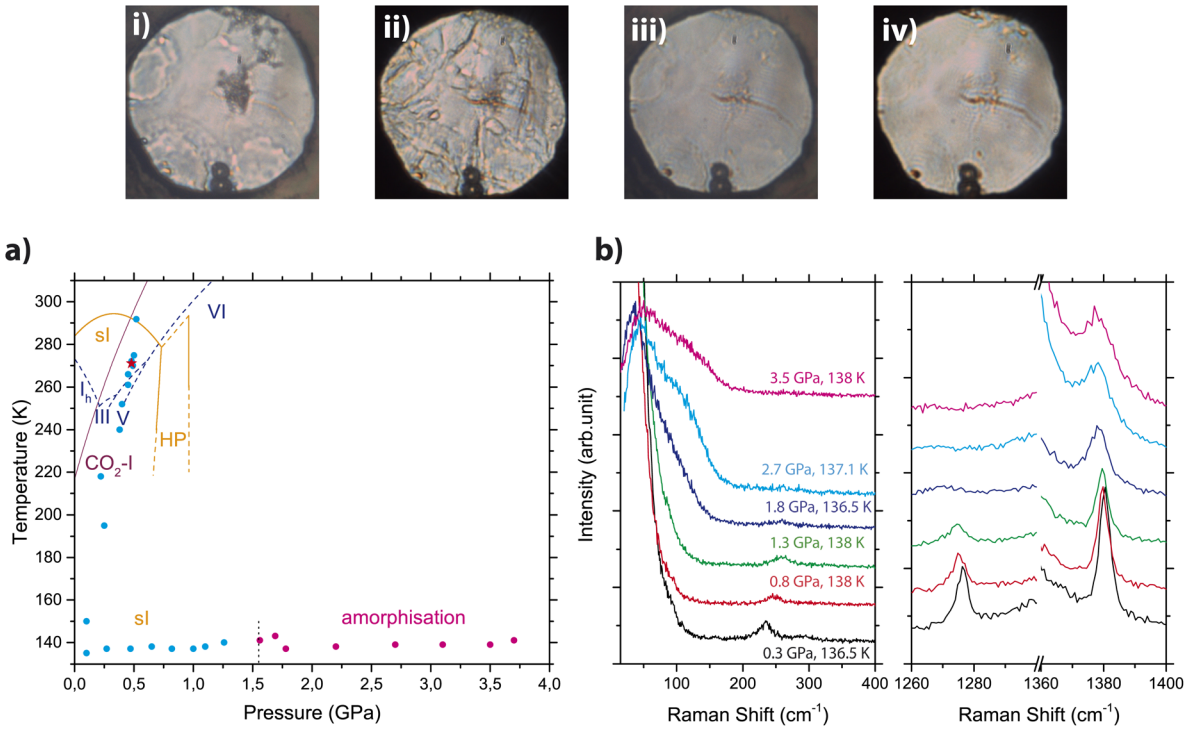

Fig. 2 Top: Microphotographs of the sample during the isothermal compression of CO_2 clathrate hydrate. (i) 0.3 GPa and 140.5 K; (ii) 1.3 GPa and 139.6 K; (iii) 1.8 GPa and 136.8 K; (iv) 3.6 GPa and 139.3 K. Bottom: Panel (a) phase diagrams of CO_2 clathrate hydrate (orange, constructed from data of Bollengier *et al.*[51]), H_2O (blue dashed lines, from ref. 56) and CO_2 (solid purple line, from ref. 57). The circles indicate experimental points taken upon cooling and isothermal compression in the sI (cyan) and amorphous (magenta) phases. Panel (b) Raman spectra acquired on the sample upon isothermal compression in the low frequency region (left) and in the Fermi resonance region (right) under corresponding *p*,*T* conditions. Spectra are vertically shifted for the sake of clarity.

Fig. 2 reports a sequence of Raman spectra acquired during the low temperature compression, together with a phase diagram showing the actual *p*,*T* points at which the sample was investigated and a selection of microphotographs acquired at various stages. The lattice phonon band assigned to the sI CO_2 clathrate hydrate progressively weakens upon compression (panel b of Fig. 2) to vanish above 1.6 GPa (where the CO_2 clathrate hydrate was reported to decompose – from literature data[50–52]). Simultaneously, the low frequency region of the spectrum changed drastically with the appearance of an unstructured band which intensifies and broadens upon compression. The progressive weakening of the lattice phonon mode of the clathrate hydrate is accompanied by an evident broadening and weakening of the Fermi resonances bands, and especially of Ω^- that vanishes around 1.5 GPa. With regard to the fate of CO_2 clathrate hydrate upon low temperature compression, no clear indication of any phase transition from the sI phase to the suggested HP phase was obtained in our experiments as instead reported by Hirai *et al.*[50] (see Fig. SI-1 for more details). This led us to consider that, at least at 130 K, the CO_2 clathrate hydrate remains in its sI structure up to a maximum pressure of about 1.6 GPa, where amorphisation takes place. This structural change is also highlighted by a clear modification of the sample appearance (see microphotographs in Fig. 2), which transforms from a grained appearance (i and ii) to a progressively more uniform and transparent one (iii and iv).

In the last step of the *p*,*T* cycle, the sample isothermally compressed up to 4 GPa at about 130 K was isobarically heated back to room temperature. Fig. 3 reports the sequence of Raman spectra acquired during isobaric heating, together with a phase diagram showing the actual *p*,*T* points measured and a selection of the most significant microphotographs taken on the sample.

The first important spectral modification in the sample is observed around 200 K, where a broad and initially weak band appears at about 1050 cm^{-1}. The intensity of this band increases upon heating, becoming clearly visible at about 206 K (green trace in Fig. 3, panel b). This band is suggestive of the formation of H_2CO_3 molecules, and it is by far the most intense band in the carbonic acid polymorphs spectra,[31,32,48] assigned to the C–O/C=O stretching mode. This interpretation is further supported by the simultaneous disappearance of the CO_2 Fermi dyad. Significantly, together with the progressive sharpening and strengthening of the C–O/C=O stretching band, a clear weakening of the broad low frequency Raman band centred at about 100 cm^{-1} is observed. Sharp peaks emerge in this low frequency region when the temperature overcomes 273 K, attesting to the formation of an ordered lattice. The resulting spectrum perfectly agrees with that of the lattice phonons of the ε_m phase.[48] On subsequent heating to room temperature, the lattice phonon bands further sharpen, while the intense C–O/C=O stretching mode band, initially quite broad, assumes

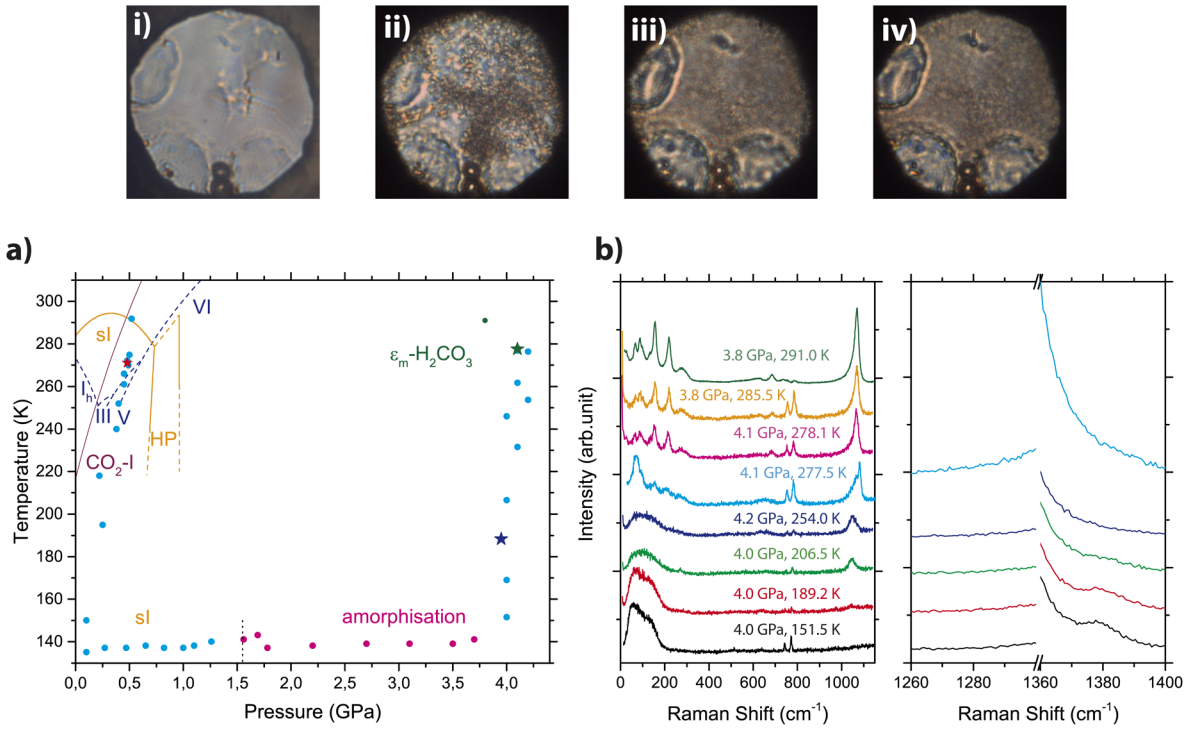

Fig. 3 Top: Microphotographs of the sample during the isobaric heating of the amorphous phase upon ε_m-H_2CO_3 synthesis. (i) 4.0 GPa and 206.5 K; (ii) 4.1 GPa and 277.5 K; (iii) 4.1 GPa and 278.1 K; (iv) 3.8 GPa and 285.5 K. Bottom: Panel (a) phase diagrams of CO_2 clathrate hydrate (orange, constructed from data of Bollengier *et al.*[51]), H_2O (blue dashed lines, from ref. 56) and CO_2 (solid purple line, from ref. 57). The circles highlight experimental points taken upon cooling and isothermal compression in the sI (cyan) and amorphous (magenta) phases and subsequent isobaric heating. The blue star marks the appearance of the band related to C–O/C=O stretching modes in H_2CO_3, while the green star marks the appearance of lattice phonon modes ascribable to ε_m-H_2CO_3. Panel (b) Raman spectra acquired on the sample upon isobaric heating in the low frequency region (left) and in the Fermi resonance region (right) under corresponding *p*,*T* conditions. The sharp doublet observable just below 800 cm^{-1} is due to the ruby fluorescence. Spectra are vertically shifted for the sake of clarity.

the shape already observed in previous experiments,[48] centred at about 1070 cm^{-1} and featuring a broad, weak low frequency shoulder. No bands are observed at room temperature in the Fermi resonance region, thus attesting to the absence of free CO_2 in the ε_m-H_2CO_3 rich portion of the sample (see panel b of Fig. 3). The quality of the spectrum (further shown in Section SI-2 of SI and particularly in Fig. SI-2 and SI-3) is so high that a phonon mode, not reported previously,[48] has been observed at 26.9 cm^{-1}. In addition, the spectral region between 600 and 900 cm^{-1} is well resolved, making it possible to follow the pressure evolution of the three internal modes detected here (see Fig. SI-3). As a final consideration, the nucleation of ε_m-H_2CO_3 is clearly visible also from the visual observation of the sample (see microphotographs on top of Fig. 3): upon progressive heating, the sample transforms from opaque (i) to grainy when the formation of the crystal begins (ii) (at 4.1 GPa and 277.5 K), becoming evidently polycrystalline once it reaches ambient temperature (iii and iv).

These results have been reproduced in all the experiments we performed and where the clathrate hydrate was successfully synthesised. As described in detail in Section SI-3 of the SI, the attainment of the clathrate hydrate was influenced by the eventual excess of CO_2 which seems to make the hydrate nucleation more and more difficult with increasing pressure. This aspect is particularly relevant because the formation of CO_2 clathrate hydrate is needed to produce crystalline ε_m-H_2CO_3 at the end of the *p*,*T* cycle. In fact, over a number of experiments, only the ones where CO_2 clathrate hydrate was efficiently synthesised at low temperature and low pressure ended in the formation of crystalline ε_m-H_2CO_3 (see Fig. 3 and SI-7). In contrast, when we subjected intimately mixed CO_2 and H_2O ices to the same *p*,*T* cycle, we only observed the appearance of the band related to the C–O/C=O stretching mode of the H_2CO_3 molecules and with a very modest intensity (see Fig. SI-8), thus indicating a minimal formation of H_2CO_3 molecules likely limited to the boundaries between CO_2 and H_2O grains.

The Raman results have been complemented and fully confirmed by a synchrotron diffraction experiment (Xpress – ELETTRA, $\lambda = 0.49568$ Å) where we followed exactly the same *p*,*T* path as in the Raman experiments. Once the CO_2 clathrate hydrate was synthesised at about 0.4 GPa, we cooled it isobarically down to 135 K, then we compressed it isothermally up to 4 GPa, and finally heated it isobarically up to ambient temperature. Representative XRD patterns acquired on the sample during the entire cycle are presented in Fig. 4. The diffraction pattern of the sI phase is observed almost unaltered up to 1.6 GPa, the same pressure range where we also detected the lattice phonon of the clathrate hydrate. At this pressure, the

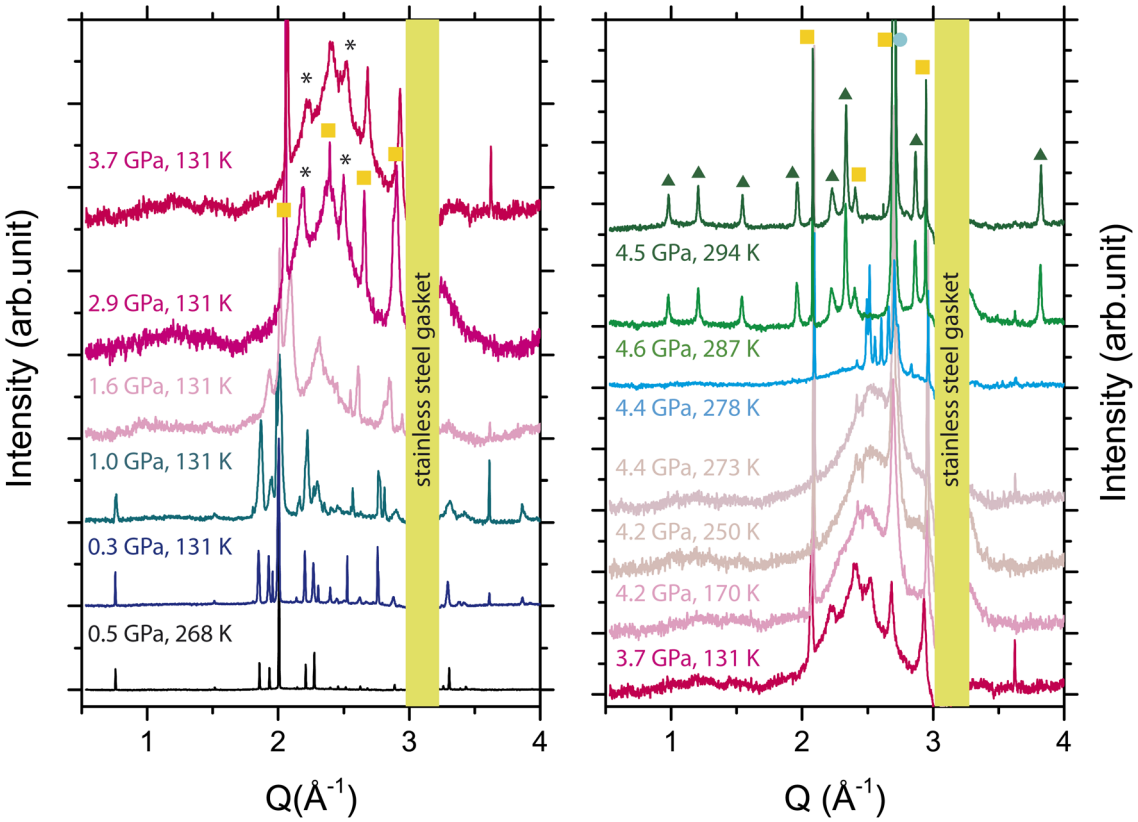

Fig. 4 Azimuthally averaged XRD patterns acquired during the isobaric (0.5–0.3 GPa) cooling of the CO_2 clathrate hydrate and subsequent isothermal (131 K) compression up to about 4 GPa (left panel) and along the isobaric (4–4.5 GPa) heating up to ambient temperature (right panel). Yellow squares, cyan circles and green triangles, respectively, mark Bragg peaks from CO_2-I, ice-VII and ε_m-H_2CO_3. The two additional peaks visible in the patterns recorded at 2.9 and 3.7 GPa (131 K) and highlighted by black asterisks are likely remnants of the hydrate crystal phase. The peaks in the first pattern on the bottom of the left panel (black curve, 0.5 GPa at 268 K) were indexed as the sI phase of CO_2 clathrate hydrate.[71] Upon compression, Bragg peaks from CO_2-I and, occasionally, ice-II become visible. The yellow highlighted area covers the Q region where the very intense diffraction signal from the gasket material (stainless steel) was dominating the diffraction patterns. The background has been subtracted to remove the contribution from the Kapton windows of the cryostat.

diffraction peaks of CO_2 clathrate hydrate are replaced by a weak, broad and unstructured band centred at a *d*-spacing of about 2.7 Å, which nicely resembles the FDP (First Diffraction Peak) of amorphous ices, especially VHDA (Very High Density Amorphous), at 85 K,[58,59] thus supporting the clathrate hydrate amorphisation. Clathrate hydrate amorphisation has been reported for several systems: THF,[60,61] dioxolane,[62] cyclobutanone,[63] CH_4,[64,65] C_2H_6,[65] Ar and Xe.[66] Molecular dynamics simulations have provided structural models for some of these systems[61,67] and also for CO_2 hydrate,[68] for which no experimental data have been available so far. All these studies consistently indicate that guest molecules remain nearly localized in their clathrate positions, preserving short- and medium-range correlations and preventing the decomposition of the mixed amorphous ice. This feature is crucial for the reaction, as it maintains a homogeneous distribution of CO_2 molecules within the water ice matrix. The broad FDP is observed substantially unaltered during the heating cycle up to 277 K, where seven sharp peaks suddenly emerge in the 2.65–2.19 Å *d* range. The appearance of these sharp peaks, together with the simultaneous reduction in intensity of the broad amorphous peak, suggests the crystallization of at least part of the sample. All emerging peaks fall within the FDP, closely mirroring what is observed in pure ice,[59,69,70] possibly indicating the formation of metastable forms of pure or mixed ice. At 278 K, the same temperature at which the lattice phonon modes appeared in the Raman spectrum, the diffraction pattern drastically changes with the appearance of the characteristic diffraction peaks of ε_m-H_2CO_3 and the disappearance of all the other features with the only exception of those relative to CO_2-I. A detailed view of the changes occurring between 273 and 287 K is reported in Fig. SI-9 in the SI.

Another important issue concerns the stability of CO_2 clathrate hydrate upon compression at low temperature. The transition from the sI to the high pressure (HP) structure is reported in the range of 0.4–0.7 GPa,[50–52,72] even though only Hirai *et al.*[50] reports this transition below 150 K. We did not observe any indication of a phase transition occurring between 0.1 and 1.6 GPa during the low temperature (130 K) compression neither spectroscopically nor from X-ray diffraction. On the other hand, a clear change in the Raman spectra in the visual aspect and in the diffraction pattern of the compressed samples

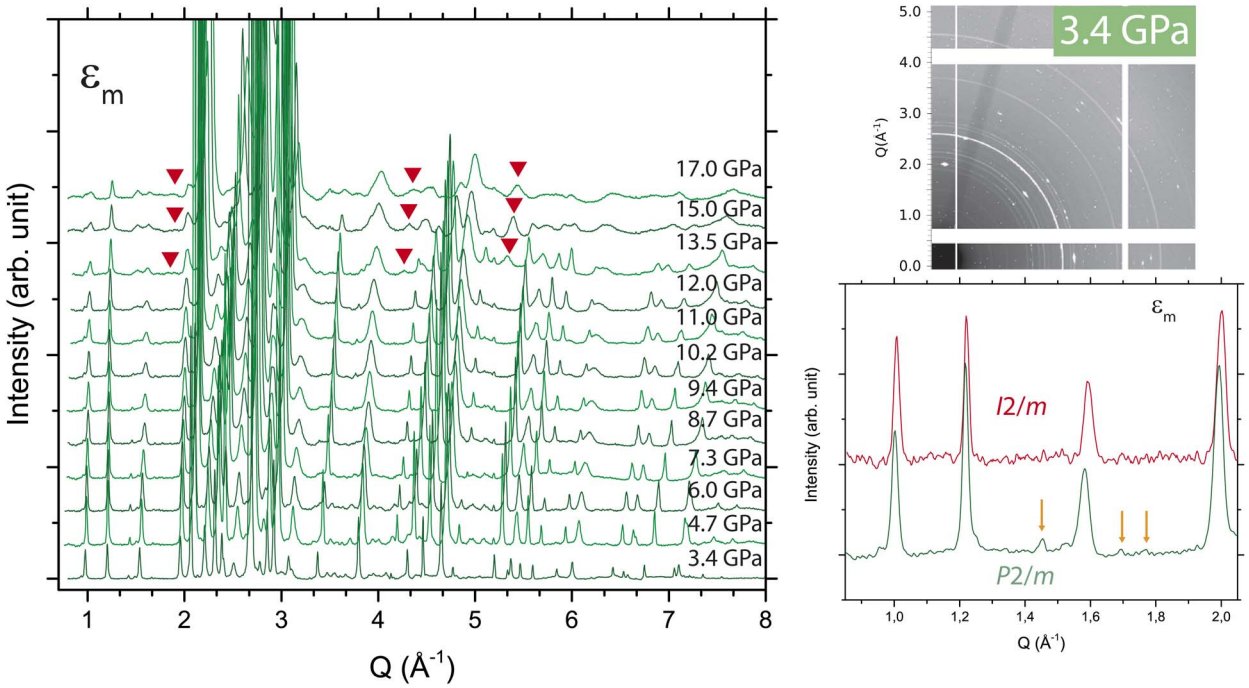

Fig. 5 Left panel: Azimuthally averaged XRD patterns acquired (λ = 0.3738 Å) on ε_m-H_2CO_3 along a room temperature compression up to 17 GPa. The patterns have been normalised to the most intense peak and vertically translated for the sake of clarity. The red triangles highlight regions in the XRD patterns where extra peaks are observed above 12 GPa. Right panel: Portion of a 2D diffraction image from the ε_m-H_2CO_3 at 3.4 GPa, highlighting the good quality of the ε_m-H_2CO_3 powder and a detail of the diffraction patterns where the extra peaks related to the *P*2/*m* unit cell are highlighted by orange arrows.

was observed above 1.6 GPa. In the Raman spectrum, the CO_2 clathrate hydrate lattice phonon mode progressively disappeared and, contextually, a broad and non-structured band arose at a very low frequency, blue-shifting upon increasing pressure. In the diffraction pattern, these spectroscopic changes combine with the appearance of a broad feature common in amorphous ices. Therefore, while no indication of a phase transition occurring in the clathrate hydrate has been obtained, it is evident that the low temperature compression leads to an amorphous compound, likely characterised by a short range order as attested by the broad structure (density of states) in the low frequency range of the Raman spectrum. The pressure induced amorphisation (PIA) of clathrate hydrate is largely studied, especially for its link to the conversion of ice-I_h into low-density or high-density amorphous phases (LDA or HDA),[61,62,65–67,73–75] and it is usually reported in clathrate hydrates along low temperature compression, at various pressures depending on the hosted molecules.[65,66] In the course of PIA, a collapse of the water cages is observed, somehow preserving a spatial correlation among the guest molecules.[61,66,74] As a matter of fact, while H_2CO_3 molecules also form when the solid CO_2–H_2O mixture is compressed, thus indicating that density rules the reactivity, ε_m-H_2CO_3 efficiently nucleated only where the crystals of CO_2 clathrate hydrate were previously observed. This suggests that a pre-existing ordering of CO_2 and H_2O molecules plays a significant role in favouring a periodic distribution of H_2CO_3 molecules needed to obtain the ε_m structure upon temperature annealing.

The process leading from CO_2 clathrate hydrate to the formation of crystalline carbonic acid can be therefore divided into two distinct steps. The first step regards the formation of H_2CO_3 molecular units through the density-driven reaction between CO_2 and H_2O molecules, as obtained from the low temperature compression of CO_2 clathrate hydrate. This step occurs both in the amorphised clathrate hydrate and at the grain boundaries of crystalline ice and CO_2. In the second step, which is observed only when the clathrate hydrate has been efficiently crystallised, a temperature driven long-range order is established among the H_2CO_3 molecules, thanks to the increasing amplitude and population of the phonon lattice modes, shaping the actual crystal structure. This also explains why, in the absence of CO_2 clathrate hydrate, only a few and isolated H_2CO_3 molecules are obtained (see Fig. SI-8): H_2CO_3 molecules form where CO_2 and H_2O are in close contact, but the lack of a fine mixing of the two reactants prevents their organisation into an ordered crystalline structure.

The ε_m phase of H_2CO_3

The pressure evolution of ε_m samples, synthesised according to the procedure described above, has been characterised by synchrotron X-ray diffraction (ESRF, λ = 0.3738 Å). Fig. 5 reports a sequence of XRD patterns acquired on the sample during a room temperature compression up to 17 GPa.

Exploiting the small spot sizes (varying between 0.7 and 3.0 μm) available at the ID27 beamline at ESRF,[76] we measured XRD patterns across a square mesh on the sample. The patterns were

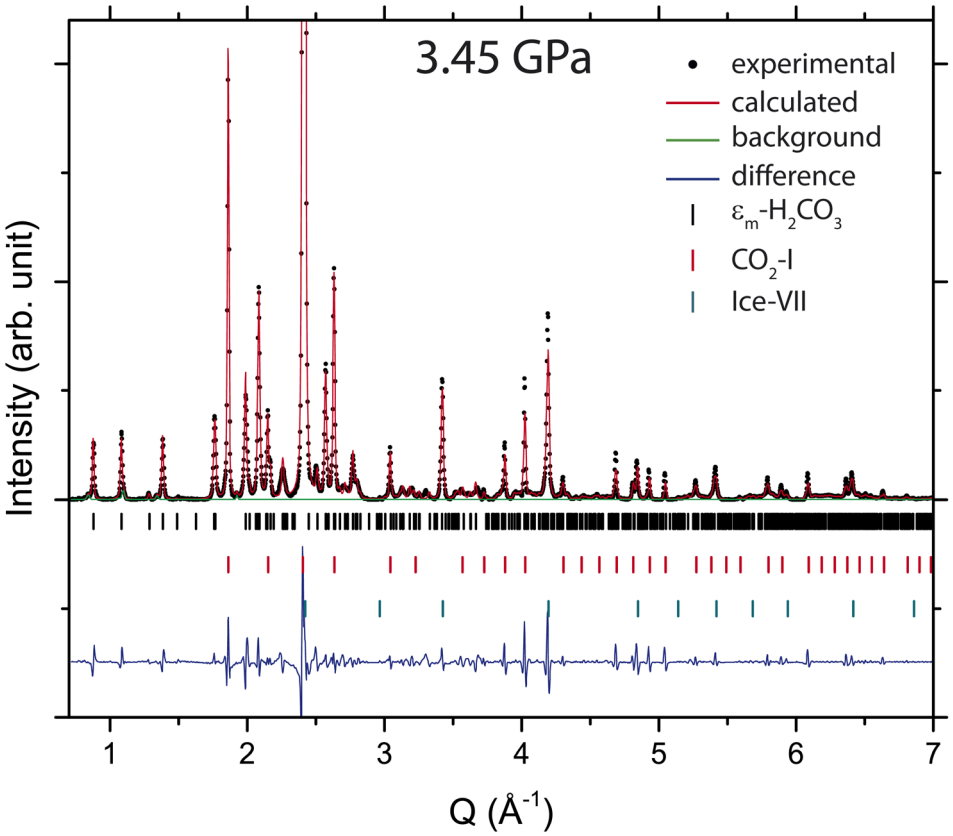

Fig. 6 Example of Le Bail refinement performed on the powder pattern of ε_m-carbonic acid in the DAC at 3.45 GPa ($\lambda = 0.3738$ Å). The cell was previously indexed to a *P*2/*m* symmetry using GSAS-II, and Le Bail refinement was performed using this monoclinic unit cell. The obtained cell parameters at 3.45 GPa are $a = 2.8671(3)$ Å, $b = 10.418(1)$ Å, $c = 12.691(2)$ Å, $\beta = 139.9781(8)°$ and $V = 243.77(5)$ Å^3. The black ticks indicate the expected reflections of the *P*2/*m* unit cell (Miller indices, peak positions and relative intensities are tabulated in Section SI-5 of the SI). Red and cyan ticks mark the expected reflections of CO_2-I and ice-VII, respectively.

textured, which shows that the sample is polycrystalline with fine grains of sizes in the order of 1 μm (see the portion of 2D diffraction image presented on the top of right panel of Fig. 5). Analysing the powder patterns over a number of different runs, we detected some differences among various ε_m samples, as shown in Fig. 5 (bottom right panel). As it can be easily observed, within a pattern nicely resembling that of ε_m structure,[48] some weak extra peaks (highlighted by arrows in the right panel of Fig. 5) appear. The XRD patterns where these peaks were not present have been indexed to a monoclinic unit cell (*I*2/*m*) using GSAS-II[77] and then analysed through the Le Bail method. The patterns where the extra peaks were observed have been assigned instead to a *P*2/*m* unit cell. Fig. 6 presents an example of Le Bail extraction of a *P*2/*m* low pressure pattern.

In the runs characterised by excellent powder quality, only reflections associated with the *I*2/*m* crystal phase were observed at lower pressures (up to 5.5 GPa). Upon increasing the pressure, additional low-intensity peaks attributable to the *P*2/*m* phase became visible. At higher pressures, however, these peaks disappeared in the background noise due to the overall peak broadening. The only difference between these two structures lies in the body centering of the *I*2/*m* unit cell, thus the observation of a *P*2/*m* structure can be related to a slight molecular displacement. For this reason, we can explain the concurrent presence of these crystal structures as due to the introduction of an external stress (*i.e.*, compression). Since one of the samples predominantly exhibited the *I*2/*m* phase at low pressure and only barely detectable *P*2/*m* reflections at intermediate pressures, we indexed this run as *I*2/*m*, considering the former as a trace contaminant. In contrast, the other sample displayed intense and sharp reflections corresponding to the *P*2/*m* phase, and was therefore successfully indexed in this symmetry. In spite of these differences in phase assignment, both compression experiments yielded nearly identical results for the pressure evolution of the unit-cell volume and lattice parameters. In Fig. 7, we present the evolution with pressure of the refined lattice parameters *a*, *b*, *c*, and β and the unit cell volume *V*. The first thing to be noticed is that, if compared to the pressure evolution of the cell parameters obtained for the ε-carbonic acid and reported elsewhere,[48] the lattice parameters do not show any discontinuity upon increasing pressure in correspondence to the pattern changes observed for the stable polymorph ε above 9 GPa. No phase transition was observed, but a general worsening of crystal quality upon compression. The collected XRD patterns underwent a clear broadening accompanied by the appearance of a few extra peaks above 12 GPa, as it can be seen for *Q* values of about 1.9, 4.5 and 5.3 Å^{-1} (see Fig. 5). While the β angle value is not much affected by the compression, *a* and *c* unit cell parameters tend to vary slightly more than the

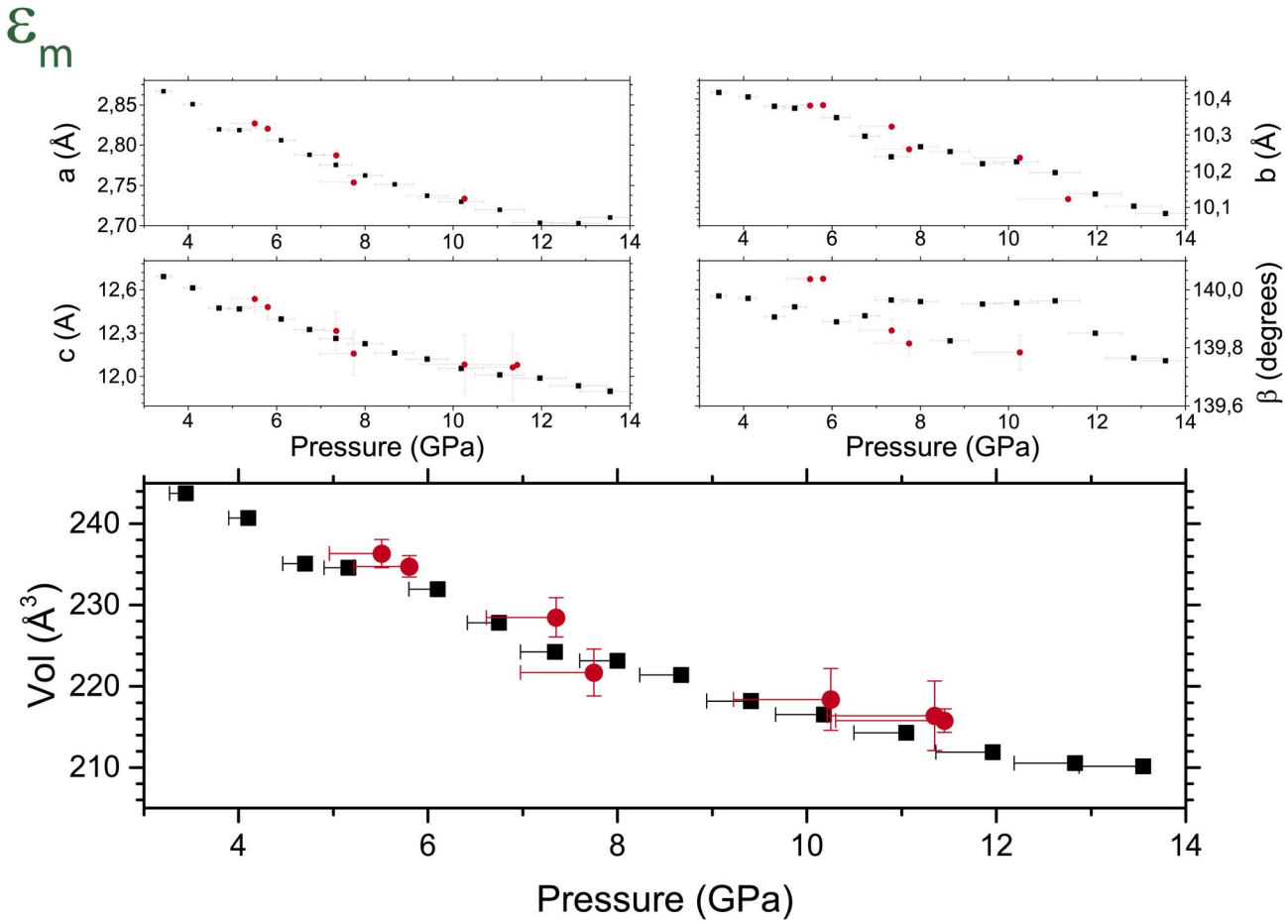

Fig. 7 Top panels: *a*, *b*, *c* and *β* lattice cell parameters of ε_m-carbonic acid upon compression. Bottom panel: Unit cell volume of ε_m-carbonic acid as a function of pressure. Red dots and black squares are related to the cell parameters, respectively, from *I*2/*m* and *P*2/*m* unit cell symmetries, as obtained through Le Bail refinements and referring to different experimental runs (see the text). The error on the computed parameters, when nonvisible, is smaller than symbols. Pressure has been measured using the Re equation of state.[78] Refinement data are available for the runs in Section SI-5 and Tables SI-1 and SI-2.

b parameter (see also Fig. SI-10). The unit cell volume at 7.4 GPa is 224.2(1) Å^3, only slightly lower if compared to that measured for the ε polymorph at analogous pressure (235.14(4) Å^3). This information is of paramount importance to define the crystal structure of the metastable ε_m phase. In fact, the missed observation of high frequency –OH stretching bands, instead observed in the ε phase, together with the detection of half of the lattice phonon modes of the ε phase, let hypothesise a possible anhydrous phase. Obviously, this contrasts with a volume almost identical to that of a crystal structure, ε-H_2CO_3, containing two H_2O and two H_2CO_3 molecules per cell, and it is compatible with the picture of ε_m containing disordered H_2O molecules rather than no water at all, as previously speculated.[48] The Le Bail extraction of the patterns becomes increasingly difficult above 11.6 GPa, likely also because of the sluggish I–III phase transition of excess CO_2 present in the sample.

Conclusions

In this study, we addressed a fundamental problem in solid-state chemistry concerning the pressure- and temperature-induced heterogeneous solid–solid reactions in simple ices. Specifically, we investigated the conversion of CO_2 clathrate hydrate into a hydrated polymorph of carbonic acid through a low temperature (100–200 K) compression (<4 GPa). The choice of these species directly stems from their relevance in astrochemistry since the *p*,*T* conditions where the formation of H_2CO_3 polymorphs have been observed are close to the thermodynamic conditions characterizing the surfaces and first crustal layers of several icy satellites and planets where CO_2 and H_2O can be found. By simulating a subduction process of the clathrate through compression at temperatures typical of the icy surfaces of outer solar system planets and satellites, we observed the transformation of CO_2 clathrate hydrate into the ε_m phase of carbonic acid.

This phase was recently and accidentally discovered, along with other hydrated polymorphs of carbonic acid, following the cold loading of CO_2 clathrate in a diamond anvil cell.[48] In this work, we attempted to reproduce the presumed *p*,*T* pathway followed during the cold loading in order to understand the reactive steps leading to the H_2CO_3 crystalline polymorphs formation. To do that, we first synthesised the clathrate in the cell, which was then isobarically cooled at low pressure, and

subsequently compressed at low temperatures, monitoring all these phases by both Raman spectroscopy and X-ray diffraction. In doing so, we were able to reveal the mechanism by which the transformation occurred. First and foremost, the presence of clathrate is essential for the final formation of the crystalline phase of carbonic acid. When a mixture of ice and CO_2 is used instead, only a small quantity of carbonic acid molecules is observed likely forming at the grain boundaries of the two species. The transformation occurs in two steps. In the first step, driven by pressure alone, molecule formation is observed at temperatures around 200 K and pressures between 3 and 4 GPa. The intensities of the Raman bands associated with the internal modes of carbonic acid increase with temperature, indicating the progress of the chemical transformation. The second step, occurring around 273 K, involves the formation of the crystalline lattice, as revealed by the appearance and subsequent intensification of the characteristic diffraction peaks of the ε_m phase and by the relative lattice modes. The necessity of using clathrate hydrate as the starting material arises from the fact that only in this way the reacting mixture contains an almost homogeneous and periodic distribution of CO_2 molecules, which appears as a prerequisite for the subsequent ε_m crystal formation. It is also important to highlight that the cold compression of clathrate does not show evidence of the sI–HP transition previously reported below 1 GPa. Conversely, the sI phase is stable or metastable up to 1.6 GPa where the amorphisation of the clathrate is observed. The characteristics of this amorphous phase are extremely intriguing because a strong and unstructured Raman intensity at low frequencies suggests a short-range order, a property that could be crucial for the lattice ordering following the chemical reaction.

Finally, the ε_m-H_2CO_3 phase obtained in these experiments was further characterised as a function of pressure through synchrotron X-ray diffraction. The unit cell can be indexed at lower pressures as monoclinic $I2/m$, eventually distorted to $P2/m$ upon compression. The equation of state and lattice parameters were obtained through Le Bail refinement. The volume of this metastable phase is almost identical to that of the thermodynamically stable ε phase, thus indicating that ε_m also features two disordered water molecules per cell, thus representing a kinetically trapped intermediate phase.

Besides the implications in fundamental chemistry, the results of this study can be highly significant from the perspective of modelling the composition and the chemistry occurring in remote icy worlds also in the absence of irradiation, thus expanding beyond the photochemistry of cold surfaces the processes to be considered in order to increase our understanding of the chemistry occurring in these extraterrestrial environments.

Author contributions

Selene Berni: investigation, formal analysis, validation, writing – review & editing. Demetrio Scelta: conceptualization, investigation, formal analysis, validation, writing – original draft, writing – review & editing, supervision. Sebastiano Romi: investigation, formal analysis, validation, writing – review & editing. Samuele Fanetti: investigation, writing – review & editing. Frederico Alabarse: investigation, writing – review & editing. Bjorn Wehinger: investigation, writing – review & editing. Roberto Bini: conceptualization, investigation, formal analysis, validation, writing – original draft, writing – review & editing, resources, funding acquisition, supervision.

Conflicts of interest

There are no conflicts to declare.

Data availability

The crystallographic data (XRD) collected at the ID27 ESRF Beamline (experiment CH-7025) are available at the following DOI: proposal **https://doi.org/10.15151/ESRF-ES-1554170001**. All other data (in house and Elettra XRD data, and Raman data) will be available upon reasonable request on the author.

Supplementary information is available. See DOI: **https://doi.org/10.1039/d5sc02241j**.

Acknowledgements

The authors acknowledge the funding provided by the project IPHOQS, CUP: B53C22001750006. The authors also acknowledge the financial support provided under the National Recovery and Resilience Plan (NRRP), Mission 4, Component 2, Investment 1.1, Call for tender no. 104 published on 2/2/2022 by the Italian Ministry of University and Research (MUR), funded by the European Union-NextGenerationEU, Project Title: Pressure induced photoreduction of CO_2 inside inorganic and metal organic porous materials, CUP B53D23025660001, Grant Assignment Decree No. 1384 adopted on 01/09/2023 by the Italian Ministry of Ministry of University and Research (MUR). This research has also been funded by the European Union-NextGeneration EU, within PRIN 2022, PNRR M4C2, Project E-ICES, Project Title: Probing the exotic properties of gas and ions filled ICES under extreme conditions: from planetary interiors modelling to hydrogen storage and green energy applications 2022NRBLPT, CUP B53D23004390006. This study was further supported by the Deep Carbon Observatory (DCO) initiative under the project Physics and Chemistry of Carbon at Extreme Conditions and by the Italian Ministero dell'Istruzione, dell'Università e della Ricerca (MIUR). The authors acknowledge the ESRF synchrotron for the provision of synchrotron radiation facilities (proposal CH-7025, **https://doi.org/10.15151/ESRF-ES-1554170001**) and thank B. Wehinger for his assistance in using beamline ID-27 (ESRF, Grenoble). The authors acknowledge the Elettra Sincrotrone Trieste for the provision of synchrotron radiation facilities (proposal 20245138) and thank F. Alabarse for his assistance in using beamline XPress. S. B. thanks the project CNR-FOE-LENS.

Notes and references

1 U. Marboeuf, A. Thiabaud, Y. Alibert, N. Cabral and W. Benz, *Astron. Astrophys.*, 2014, **570**, A36.

2 A. D. Fortes and M. Choukroun, *Space Sci. Rev.*, 2010, **153**, 185–218.
3 J. S. Kargel and J. I. Lunine, *Solar System Ices: Based on Reviews Presented at the International Symposium "Solar System Ices" held in Toulouse*, France, on March 27–30, 1995, pp. 97–117.
4 D. Bockelée-Morvan and N. Biver, *Philos. Trans. R. Soc., A*, 2017, **375**, 20160252.
5 N. Schorghofer, J.-P. Williams, J. Martinez-Camacho, D. A. Paige and M. A. Siegler, *Geophys. Res. Lett.*, 2021, **48**, e2021GL095533.
6 M. N. De Prá, E. Hénault, N. Pinilla-Alonso, B. J. Holler, R. Brunetto, J. A. Stansberry, A. C. de Souza Feliciano, J. M. Carvano, B. Harvison, J. Licandro, *et al.*, *Nat. Astron.*, 2024, 1–10.
7 W. Grundy, L. Young and E. Young, *Icarus*, 2003, **162**, 222–229.
8 B. J. Buratti, D. P. Cruikshank, R. H. Brown, R. N. Clark, J. M. Bauer, R. Jaumann, T. B. McCord, D. P. Simonelli, C. A. Hibbitts, G. B. Hansen, T. C. Owen, K. H. Baines, G. Bellucci, J.-P. Bibring, F. Capaccioni, P. Cerroni, A. Coradini, P. Drossart, V. Formisano, Y. Langevin, D. L. Matson, V. Mennella, R. M. Nelson, P. D. Nicholson, B. Sicardy, C. Sotin, T. L. Roush, K. Soderlund and A. Muradyan, *Astrophys. J.*, 2005, **622**, L149.
9 E. Dartois and F. Langlet, *Astron. Astrophys.*, 2021, **652**, A74.
10 M. P. Bernstein, J. P. Dworkin, S. A. Sandford, G. W. Cooper and L. J. Allamandola, *Nature*, 2002, **416**, 401–403.
11 G. Munoz Caro, U. J. Meierhenrich, W. A. Schutte, B. Barbier, A. Arcones Segovia, H. Rosenbauer, W.-P. Thiemann, A. Brack and J. M. Greenberg, *Nature*, 2002, **416**, 403–406.
12 M. Palumbo, G. Strazzulla, Y. Pendleton and A. Tielens, *Astrophys. J.*, 2000, **534**, 801.
13 T. Loerting, C. Tautermann, R. T. Kroemer, I. Kohl, A. Hallbrucker, E. Mayer and K. R. Liedl, *Angew. Chem., Int. Ed.*, 2000, **39**, 891–894.
14 K. Adamczyk, M. Prémont-Schwarz, D. Pines, E. Pines and E. T. Nibbering, *Science*, 2009, **326**, 1690–1694.
15 C. J. Bennett, C. P. Ennis and R. I. Kaiser, *Astrophys. J.*, 2014, **794**, 57.
16 B. M. Jones, R. I. Kaiser and G. Strazzulla, *Astrophys. J.*, 2014, **788**, 170.
17 G. Strazzulla, J. Brucato, G. Cimino and M. Palumbo, *Planet. Space Sci.*, 1996, **44**, 1447–1450.
18 S. Ioppolo, Z. Kaňuchová, R. L. James, A. Dawes, A. Ryabov, J. Dezalay, N. C. Jones, S. V. Hoffmann, N. J. Mason and G. Strazzulla, *Astron. Astrophys.*, 2021, **646**, A172.
19 M. L. Delitsky, D. A. Paige, M. A. Siegler, E. R. Harju, D. Schriver, R. E. Johnson and P. Travnicek, *Icarus*, 2017, **281**, 19–31.
20 M. Sanz-Novo, V. M. Rivilla, I. Jiménez-Serra, J. Martín-Pintado, L. Colzi, S. Zeng, A. Megías, Á. López-Gallifa, A. Martínez-Henares, S. Massalkhi, *et al.*, *Astrophys. J.*, 2023, **954**, 3.
21 M. L. Delitsky and A. L. Lane, *J. Geophys. Res.:Planets*, 1998, **103**, 31391–31403.
22 M. Moore and R. Khanna, *Spectrochim. Acta, Part A*, 1991, **47**, 255–262.
23 M. Moore, R. Khanna and B. Donn, *J. Geophys. Res.:Planets*, 1991, **96**, 17541–17545.
24 P. Gerakines, M. H. Moore and R. L. Hudson, *Astron. Astrophys.*, 2000, **357**, 793–800.
25 C. R. Wu, D. Judge, B.-M. Cheng, T.-S. Yih, C. Lee and W. Ip, *J. Geophys. Res.:Planets*, 2003, **108**, 5032.
26 K. P. Hand, R. W. Carlson and C. F. Chyba, *Astrobiology*, 2007, **7**, 1006–1022.
27 W. Zheng and R. I. Kaiser, *Chem. Phys. Lett.*, 2007, **450**, 55–60.
28 Y. Oba, N. Watanabe, A. Kouchi, T. Hama and V. Pirronello, *Astrophys. J.*, 2010, **722**, 1598.
29 N. Goldman, E. J. Reed, L. E. Fried, I.-F. William Kuo and A. Maiti, *Nat. Chem.*, 2010, **2**, 949–954.
30 F. Postberg, N. Khawaja, B. Abel, G. Choblet, C. R. Glein, M. S. Gudipati, B. L. Henderson, H.-W. Hsu, S. Kempf, F. Klenner, *et al.*, *Nature*, 2018, **558**, 564–568.
31 H. Wang, J. Zeuschner, M. Eremets, I. Troyan and J. Willams, *Sci. Rep.*, 2016, **6**, 19902.
32 E. H. Abramson, O. Bollengier and J. M. Brown, *Sci. Rep.*, 2017, **7**, 821.
33 M. H. Carr, M. J. Belton, C. R. Chapman, M. E. Davies, P. Geissler, R. Greenberg, A. S. McEwen, B. R. Tufts, R. Greeley, R. Sullivan, *et al.*, *Nature*, 1998, **391**, 363–365.
34 C. Ahrens, H. Meraviglia and C. Bennett, *Geosci.*, 2022, **12**, 51.
35 E. H. Abramson, O. Bollengier, J. M. Brown, B. Journaux, W. Kaminsky and A. Pakhomova, *Am. Mineral.*, 2018, **103**, 1468–1472.
36 W. Hage, K. R. Liedl, A. Hallbrucker and E. Mayer, *Science*, 1998, **279**, 1332–1335.
37 I. Kohl, K. Winkel, M. Bauer, K. Liedl, T. Loerting and E. Mayer, *Angew. Chem., Int. Ed.*, 2009, **48**, 2690–2694.
38 J. Bernard, M. Seidl, I. Kohl, K. R. Liedl, E. Mayer, Ó. Gálvez, H. Grothe and T. Loerting, *Angew. Chem., Int. Ed.*, 2011, **50**, 1939–1943.
39 J. Bernard, R. G. Huber, K. R. Liedl, H. Grothe and T. Loerting, *J. Am. Chem. Soc.*, 2013, **135**, 7732–7737.
40 W. Hage, A. Hallbrucker and E. Mayer, *J. Chem. Soc., Faraday Trans. 1*, 1995, **91**, 2823–2826.
41 K. Winkel, W. Hage, T. Loerting, S. L. Price and E. Mayer, *J. Am. Chem. Soc.*, 2007, **129**, 13863–13871.
42 H. P. Reisenauer, J. P. Wagner and P. R. Schreiner, *Angew. Chem., Int. Ed.*, 2014, **53**, 11766–11771.
43 E.-M. Köck, J. Bernard, M. Podewitz, D. F. Dinu, R. G. Huber, K. R. Liedl, H. Grothe, E. Bertel, R. Schlögl and T. Loerting, *Chem. Eur J.*, 2020, **26**, 285–305.
44 S. Benz, D. Chen, A. Möller, M. Hofmann, D. Schnieders and R. Dronskowski, *Inorganics*, 2022, **10**, 132.
45 L. J. Conway, C. J. Pickard and A. Hermann, *Proc. Natl. Acad. Sci. U. S. A.*, 2021, **118**, e2026360118.
46 A. S. Naumova, S. V. Lepeshkin, P. V. Bushlanov and A. R. Oganov, *J. Phys. Chem. A*, 2021, **125**, 3936–3942.
47 G. Saleh and A. R. Oganov, *Sci. Rep.*, 2016, **6**, 324816.

48 S. Berni, D. Scelta, S. Romi, S. Fanetti, F. Alabarse, M. Pagliai and R. Bini, *Angew. Chem., Int. Ed.*, 2024, **63**, e202403953.
49 D. Scelta, M. Ceppatelli, R. Ballerini, A. Hajeb, M. Peruzzini and R. Bini, *Rev. Sci. Instrum.*, 2018, **89**, 053903.
50 H. Hirai, K. Komatsu, M. Honda, T. Kawamura, Y. Yamamoto and T. Yagi, *J. Chem. Phys.*, 2010, **133**, 124511.
51 O. Bollengier, M. Choukroun, O. Grasset, E. Le Menn, G. Bellino, Y. Morizet, L. Bezacier, A. Oancea, C. Taffin and G. Tobie, *Geochem. Cosmochim. Acta*, 2013, **119**, 322–339.
52 B. Massani, C. Mitterdorfer and T. Loerting, *J. Chem. Phys.*, 2017, **147**, 134503.
53 D. Scelta, S. Fanetti, S. Berni, M. Ceppatelli and R. Bini, *J. Phys. Chem. C*, 2022, **126**, 19487–19495.
54 F. Bogani and P. R. Salvi, *J. Chem. Phys.*, 1984, **81**, 4991–5001.
55 R. Bini, P. Salvi, V. Schettino, H.-J. Jodl and N. Orlic, *J. Mol. Struct.*, 1992, **266**, 165–170.
56 M. Choukroun and O. Grasset, *J. Chem. Phys.*, 2007, **127**, 124506.
57 V. M. Giordano, F. Datchi and A. Dewaele, *J. Chem. Phys.*, 2006, **125**, 054504.
58 R. J. Nelmes, J. S. Loveday, T. Strässle, C. L. Bull, M. Guthrie, G. Hamel and S. Klotz, *Nat. Phys.*, 2006, **2**, 414–418.
59 C. Lin, X. Yong, J. S. Tse, J. S. Smith, S. V. Sinogeikin, C. Kenney-Benson and G. Shen, *Phys. Rev. Lett.*, 2017, **119**, 135701.
60 Y. Suzuki, *Phys. Rev. B:Condens. Matter Mater. Phys.*, 2004, **70**, 172108.
61 P. H. B. B. Carvalho, A. Mace, C. L. Bull, N. P. Funnell, C. A. Tulk, O. Andersson and U. Häussermann, *J. Chem. Phys.*, 2019, **150**, 204506.
62 O. Andersson and Y. Nakazawa, *J. Phys. Chem. B*, 2015, **119**, 3846–3853.
63 O. Andersson and A. Inaba, *J. Phys. Chem. Lett.*, 2012, **3**, 1951–1955.
64 C. A. Tulk, D. D. Klug, J. J. Molaison, A. M. dos Santos and N. Pradhan, *Phys. Rev. B:Condens. Matter Mater. Phys.*, 2012, **86**, 054110.
65 N. Noguchi, Y. Shiraishi, M. Kageyama, Y. Yokoi, S. Kurohama, N. Okada and H. Okamura, *Phys. Chem. Chem. Phys.*, 2023, **25**, 22161–22170.
66 P. H. B. Brant Carvalho, A. Mace, O. Andersson, C. A. Tulk, J. Molaison, A. P. Lyubartsev, I. M. Nangoi, A. A. Leitão and U. Häussermann, *Phys. Rev. B*, 2021, **103**, 064205.
67 N. J. English and J. S. Tse, *Phys. Rev. B:Condens. Matter Mater. Phys.*, 2012, **86**, 104109.
68 P. Cao, J. Wu and F. Ning, *Phys. Chem. Chem. Phys.*, 2024, **26**, 9388–9398.
69 S. Klotz, G. Hamel, J. S. Loveday, R. J. Nelmes and M. Guthrie, *Z. Kristallogr. - Cryst. Mater.*, 2003, **218**, 117–122.
70 J. Stern and T. Loerting, *Sci. Rep.*, 2017, **7**, 3995.
71 R. W. Henning, A. J. Schultz, V. Thieu and Y. Halpern, *J. Phys. Chem. A*, 2000, **104**, 5066–5071.
72 C. A. Tulk, S. Machida, D. D. Klug, H. Lu, M. Guthrie and J. J. Molaison, *J. Chem. Phys.*, 2014, **141**, 174503.
73 O. Andersson and U. Häussermann, *J. Phys. Chem. B*, 2018, **122**, 4376–4384.
74 P. H. B. Brant Carvalho, P. I. R. Moraes, A. A. Leitão, O. Andersson, C. A. Tulk, J. Molaison, A. P. Lyubartsev and U. Häussermann, *RSC Adv.*, 2021, **11**, 30744–30754.
75 O. Andersson, P. H. B. B. Carvalho, U. Häussermann and Y.-J. Hsu, *Phys. Chem. Chem. Phys.*, 2022, **24**, 20064–20072.
76 M. Mezouar, G. Garbarino, S. Bauchau, W. Morgenroth, K. Martel, S. Petitdemange, P. Got, C. Clavel, A. Moyne, H.-P. Van Der Kleij, A. Pakhomova, B. Wehinger, M. Gerin, T. Poreba, L. Canet, A. Rosa, A. Forestier, G. Weck, F. Datchi, M. Wilke, S. Jahn, D. Andrault, L. Libon, L. Pennacchioni, G. Kovalskii, M. Herrmann, D. Laniel and H. Bureau, *High Press. Res.*, 2024, **44**, 171–198.
77 B. H. Toby and R. B. Von Dreele, *J. Appl. Crystallogr.*, 2013, **46**, 544–549.
78 S. Anzellini, A. Dewaele, F. Occelli, P. Loubeyre and M. Mezouar, *J. Appl. Phys.*, 2014, **115**, 043511.